JOURNAL OF GEOPHYSICAL RESEARCH, VOL. 113, B12304, doi:10.1029/2007JB005336, 2008

A global search for stress shadows

Ellen P. Mallman[1] and Tom Parsons[2]

Received 17 August 2007; revised 26 July 2008; accepted 17 September 2008; published 11 December 2008.

[1] Debate continues regarding the relative proportion of earthquakes triggered by passing seismic waves versus static stress changes from a main shock. Static stress changes are expected to have long-term effects on earthquake probabilities, whereas dynamic stress changes due to the passing of seismic waves should not. Both mechanisms are expected to raise seismicity rates in some areas, but only static stress change calculations predict rate decrease shadows. Thus, identification of post-main-shock earthquake suppression is diagnostic of a static stress change process. We note that in principle, static stress change theory predicts suppression of particular earthquake mechanisms in a shadow zone rather than an overall rate reduction. A stress shadow can therefore be characterized by a change in the average earthquake focal mechanism before and after a main shock that results from suppression of a given mechanism type. We examined average mechanisms from ±2° radii and 5-year periods before and after 119 $M_s \geq 7$ main shock earthquakes drawn from the Harvard Centroid Moment Tensor (CMT) catalog. Significant average mechanism changes caused by earthquake suppression were found in only two cases. However, by stacking the data, we were able to resolve statistically significant suppression of particular post-main-shock focal mechanisms. This indicates that, while static stress shadows are subtle, they are indeed present in the global catalog.

Citation: Mallman, E. P., and T. Parsons (2008), A global search for stress shadows, *J. Geophys. Res.*, *113*, B12304, doi:10.1029/2007JB005336.

1. Introduction

[2] Earthquakes modify stress in the crust surrounding a main shock rupture, and are expected to change the seismicity rate accordingly, which has implications for future earthquake probabilities and hazard modeling [*Working Group on California Earthquake Probabilities*, 2003]. Dynamic stresses induced by the passage of seismic waves [*Belardinelli et al.*, 1999; *Cotton and Coutant*, 1997; *Gomberg et al.*, 2003; *Kilb et al.*, 2000], or static stresses induced by fault offset [*Das and Scholz*, 1981; *King et al.*, 1994; *Stein and Lisowski*, 1983; *Yamashina*, 1978] are both suggested sources of near-field earthquake triggering. A key difference between the two triggering processes is that static stress changes caused by M > 7 earthquakes are expected to reduce stress, and hence suppress seismicity, in a relatively large volume of the surrounding crust [*Harris and Simpson*, 1998; *Parsons*, 2002]. This phenomenon of stress-induced seismicity rate decrease, such as the one observed following the 1906 San Francisco earthquake in California [*Stein*, 1999] is commonly known as a *stress shadow* [*Harris and Simpson*, 1998]. While this decrease in seismicity following large main shocks is predicted by static stress change models, some researchers have failed to show correlations between modeled stress decreases and observed seismicity rate changes [*Felzer and Brodsky*, 2005; *Mallman and Zoback*, 2007]. A possible explanation for the lack of resolvable decreases in seismicity rate following M > 7 earthquakes is that earthquakes triggering is dominated by the dynamic process as opposed to static stress changes [*Felzer et al.*, 2004; *Felzer and Brodsky*, 2005]. While mechanisms have been proposed for dynamic stress changes to suppress some earthquakes [*Parsons*, 2005; *Richardson and Marone*, 1999], only changes in static stresses predict broad, systematic increases and decreases in seismicity rate. We propose that a lack of observable seismicity rate decreases can be explained using static stress triggering if there is systematic suppression of particular focal mechanisms after a main shock. Using this hypothesis we performed a global search for stress shadows following $M_s \geq 7$ main shocks.

1.1. Stress Shadow Definition

[3] Stress shadows have traditionally been defined as a seismicity-rate decrease that corresponds to the static stress decrease following an individual main shock. Many authors argue that a clear stress shadow followed the 1906 San Francisco earthquake [*Harris and Simpson*, 1998]. While earthquakes were triggered near the ends of the 1906 rupture [*Meltzner and Wald*, 2003], seismicity rates appear to have been reduced adjacent to the rupture; in the San Francisco Bay area, there were numerous $M > 6$ events during the 75-year period before 1906, while in the 75 years following 1906 there was only one $M > 6$ event [*Stein*, 1999]. If the change in Coulomb failure stress (CFS) is resolved on N34°W striking right-lateral planes (similar

[1]Department of Geophysics, Stanford University, Stanford, California, USA.
[2]U.S. Geological Survey MS-999, Menlo Park, California, USA.

0148-0227/08/2007JB005336$09.00

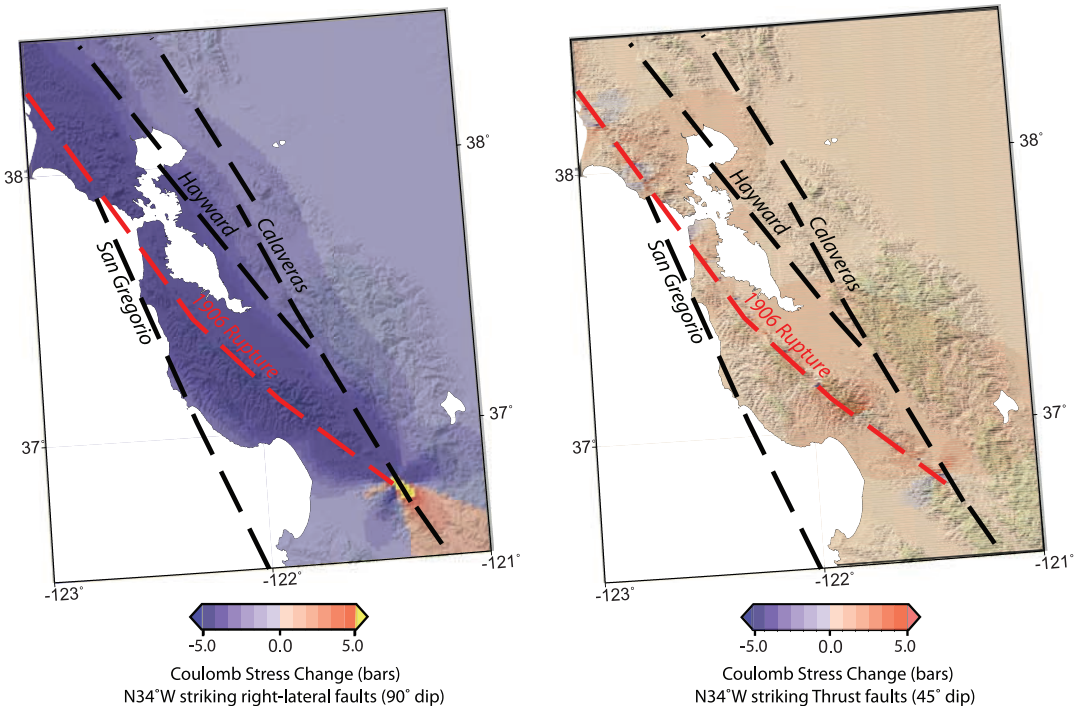

Figure 1. Changes in the Coulomb stress following the 1906 San Francisco earthquake resolved on (a) N34°W striking right-lateral planes and (b) N34°W striking dip-slip planes with a coefficient of friction of 0.4 at a depth of 5 km. Cool colors indicate a decrease in the Coulomb stress on the planes, implying a decrease in the seismic potential, while the warm colors indicate an increase in the Coulomb stress and an increase in the seismic potential. Figure 1a shows the traditional view of the stress shadow following the 1906 earthquake, but by calculating the change in stress on planes of a similar orientation to the Loma Prieta earthquake of 1989, it becomes apparent that the 1906 earthquake would have encouraged events of this mechanism.

orientation to the San Andreas Fault (SAF)) most of the region is predicted to experience a decrease in CFS, thus predicting a seismicity rate decrease similar to the observations (Figure 1a). However, not all of the active faults in the San Francisco Bay area fail in a right-lateral sense like the SAF; there are also numerous thrust faults, such as the fault that failed in the 1989 Loma Prieta earthquake [*Reasenberg and Simpson*, 1992]. If the change in CFS is resolved on thrust faults striking N34°W (the dominant orientation of the thrust faults in the coast range) there is an increase in the CFS (Figure 1b). This would predict an increase in seismicity instead of a shadow, which is predicted by the decrease in CFS seen in Figure 1a. Similar patterns are observed when resolving the change in CFS on faults of different orientations following a thrust main shock as is shown in the study of *Lin and Stein* [2004]. Another complication to attempting to match seismicity rate changes with predicted changes in CFS is the smooth nature of the main shock slip model that is generally used in the CFS modeling. The changes CFS due to the 1906 San Francisco Earthquake shown in Figure 1 are from a smoothly varying slip model, and the results would likely be quite different if the models were created with an accurate heterogeneous slip distribution. *Helmstetter and Shaw* [2006] and *Marsan* [2006] both found that heterogeneous slip could explain isolated pockets of seismicity increase within broad shadow zones. In addition to different faulting mechanisms (the sense of slip on the faults) responding differently to the same main shock there is the added complication of the difficulty in resolving seismicity rate decreases. Since seismicity is typically low before a main shock in any given year, and it is impossible to have a negative seismicity rate, stress shadows in the traditional sense are fundamentally hard to identify.

[4] Because of the difficulty in resolving traditional stress shadows and the differences in the static stress change for different faulting styles, we develop an extended definition of a stress shadow. We suggest that a static stress process is uniquely identified by a post-main shock change in average focal mechanism caused by a decrease in the seismicity rate for a given faulting regime. For example, following the 1906 San Francisco strike-slip earthquake shown in Figure 1 we would expect to see a decrease in the number of strike-slip events, but an increase in thrust events, thus satisfying the requirements of our definition.

1.2. Motivation

[5] Using this new definition for a stress shadow we examine a catalog of $M_s \geq 7$ events to see if stress shadows are present on a global scale. Working on a global scale allows for the identification of general trends instead of focusing on individual events as has been primarily done in the past [*Felzer et al.*, 2002; *Freed and Lin*, 2001; *Gomberg et al.*, 2001; *Lin and Stein*, 2004; *Ma et al.*, 2005; *Mallman and Zoback*, 2007; *Marsan and Nalbant*, 2005; *Masterlark and Wang*, 2002; *Pollitz and Sacks*, 2002; *Simpson and*

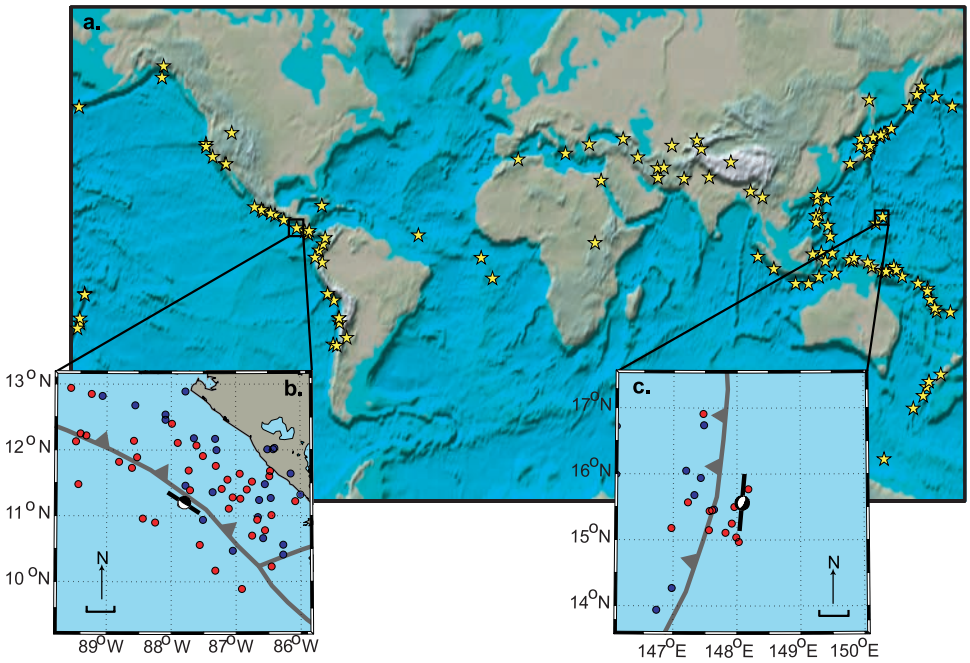

Figure 2. (a) The stars indicate the 119 $M_s \geq 7$ main shocks used in this study. (b, c) Mechanism, approximate rupture length (black line), and spatial distribution of events within ±2° before (blue) and after (red) the main shock for the two events whose statistics are shown in Figures 4 and 5. Figure 2b shows the Near Coast of Nicaragua event in Figure 5. Figure 2c shows the Mariana Islands Region event in Figure 4.

Reasenberg, 1994; *Stein*, 1999; *Toda et al.*, 1998; *Woessner et al.*, 2004; *Wyss and Wiemer*, 2000]. To search for stress shadows globally we will use the Harvard Centroid Moment Tensor (CMT) catalog between January 1977 and September 2000 to examine the average focal mechanisms and rate changes for each faulting regime following $M_s \geq 7$ main shocks.

2. Data

[6] The use of a global catalog allows us to identify processes that are active globally instead of generalizing from individual earthquakes and the large data sample implies better statistics. We stack the data to enhance small signals which allow us to detect rate and mechanism variations that would not be apparent or statistically significant for an individual event. We use the Harvard CMT global catalog between January 1977 and September 2000 for this study, the same catalog used by *Parsons* [2002] for which solutions are regularly produced for events with $M_s \geq 5.5$ [*Dziewonski et al.*, 1981]. Over the time period used in this study there were 17,402 events globally that have CMT solutions.

[7] We use the same selection criteria and thus the same subset of the CMT catalog as *Parsons* [2002] used for his global Omori-law study. We first select all $M_s \geq 7$ earthquakes as potential triggering, or stress shadow inducing events; the choice of $M_s \geq 7$ was made in advance and not changed in the course of this study. We then remove any $M_s > 7$ events within 1-spatial degree of this set as potentially triggered, even if it was larger than its predecessor following the methodology of *Parsons* [2002]. This selection process resulted in 119 events identified as main shocks (Figure 2a and Table 1). Of these 119 events 67 fall in the time window of 1985–1995 which allows an 8 year time window before and 5 year window after each main shock. These time windows before and after each main shock are necessary for the determination of rate changes and for some of the statistical tests described later. These 67 events are classified as main shocks for the remainder of this study. For each of the identified main shocks all the earthquakes in the CMT catalog within ±2° of that particular main shock are selected. By selecting events in a ±2° box we are likely selecting events outside the zone affected by changes in static stress changes, at least for some of the main shocks. However, performing the identical analyses selecting only events in a ±100km (∼1°) box (an area more likely affected by changes in static stress) produced the same results as the larger area, so we will continue using the larger area to increase the number of events for more robust statistics. For the subsequent analysis we focus on the 5 years before and after the main shock as this is the time period before the seismicity rate has returned to the background rate (see Figure 9 of *Parsons* [2002]). As illustrated in Figure 2a, the identified main shocks are dominated by circum-Pacific subduction zone events and the overall mechanism diversity in the catalog mimics the mechanism diversity observed globally. Figures 2b and 2c show the events in the 5 years before (dark blue) and after (red) for two of the identified main shocks. We will look at these two events in more detail later in the paper.

3. Methods

[8] One complication with static stress change calculations, especially when dealing with a global catalog, is the

Table 1. The 119 $M_s \geq 7.0$ Earthquakes Used in This Study

Mainshock	Date	M_s	Latitude	Longitude	Depth (km)	Mainshock Mechanism
Luzon, Philippine Islands	1977	7	16.38	122.59	35	Thrust
San Juan Province, Argentina	1977	7.4	−31.22	−67.69	20.8	Thrust
Solomon Islands	1977	7.2	−8.16	155.92	24.3	Odd
South of Sumbawa Island	1977	7.9	−11.14	118.23	23.3	Normal
South of Tonga Islands	1977	7.2	−26.1	−174.88	23.4	Normal
East coast of Honshu, Japan	1978	7.7	38.02	142.07	37.3	Thrust
Kermadec Islands	1978	7.2	−30.6	−177.02	23	Thrust
Kuril Islands	1978	7.5	44.12	149.27	28.3	Thrust
Tabas, Iran	1978	7.4	33.37	57.02	11	Thrust
Taiwan Region	1978	7.4	22.01	121.6	28.9	Thrust
Near coast of Ecuador	1979	7.1	−0.57	−80.48	25.6	Thrust
Near coast of Guerrero, Mexico	1979	7.6	17.78	−101.37	26.7	Thrust
Southeastern Alaska	1979	7.1	60.5	−141.39	18.8	Thrust
W coast of S island New Zealand	1979	7.4	−46.54	165.77	20.3	Thrust
West Irian Region	1979	7.9	−1.78	136.06	16.3	Strike slip
Algeria	1980	7.3	36.25	1.36	10.1	Thrust
Kuril Islands	1980	7	43.21	146.91	33.6	Thrust
Loyalty Islands Region	1980	7.2	−21.76	169.84	28.8	Thrust
Eureka, California	1980	7.2	41.14	−124.36	15	Strike slip
Santa Cruz Islands	1980	7.5	−12.9	166.21	43.6	Thrust
Iran	1981	7.1	30.03	57.58	15.2	Thrust
Michoacan, Mexico	1981	7.3	18.28	−102	31.8	Thrust
off coast central Chile	1981	7.2	−33.48	−73.15	40.4	Thrust
Rat Islands Aleutians	1981	7	51.52	176.1	20	Thrust
Samoa Islands	1981	7.7	−15.02	−173.16	20	Normal
Vanuatu Islands	1981	7.1	−17.34	167.27	30	Thrust
W coast of S island New Zealand	1981	7.6	−48.94	164.39	33.3	Thrust
coast of Guerrero, Mexico	1982	7	16.93	−98.32	18.6	Thrust
South of Tonga Islands	1982	7.7	−24.31	175.1	29.2	Thrust
Costa Rica	1983	7.2	8.85	−83.25	28	Thrust
Eastern Idaho	1983	7.3	44.35	−113.98	13.7	Normal
Greece	1983	7	38.13	20.38	10.1	Odd
Near coast of N Chile	1983	7.3	−27	−70.56	38.7	Thrust
Near W coast Honshu, Japan	1983	7.7	40.44	138.87	12.6	Thrust
Mid Atlantic Ridge	1984	7.1	8.36	−38.82	10	Strike slip
Kuril Islands	1984	7.1	44.17	148.62	30.6	Thrust
Near east coast Kamchatka	1984	7	56.24	163.8	21.5	Odd
Northern Sumatera	1984	7.2	−0.23	97.84	24.7	Thrust
Uzbekistan	1984	7	40.59	63.24	15	Thrust
Chile (Valparaiso)	1985	7.8	−33.92	−71.71	40.7	Thrust
New Britian Region	1985	7.1	−5.6	150.97	25.4	Strike slip
New Britian Region	1985	7.2	−4.28	152.58	31.4	Thrust
Southern Xinjiang, China	1985	7.6	39.54	75.09	15.4	Odd
Vanuatu Islands	1985	7	−14.07	166.09	24.2	Normal
West Irian Region	1985	7.1	−1.63	134.71	13.3	Strike slip
Andreanof Islands	1986	7.7	51.33	−175.43	31.3	Thrust
Kermadec Islands Region	1986	8.2	−27.93	−176.07	50.4	Odd
Papua New Guinea	1986	7.1	−4.42	143.64	99.7	Thrust
Taiwan	1986	7.8	23.97	121.85	33.2	Thrust
East Papua New Guinea	1987	7.4	−0.4	147.48	49	Strike slip
Gulf of Alaska	1987	7.6	58.17	−146	15	Strike slip
New Britian Region	1987	7.4	−6.22	149.44	47.8	Thrust
North coast of Chile	1987	7.3	−24.38	−70.93	41.9	Thrust
Oaxaca, Mexico	1987	7.7	16.22	−96.56	16.1	Thrust
Burma-China border region	1988	7.3	23	99.68	15	Strike slip
Burma-India border region	1988	7.2	25.19	94.89	100.5	Thrust
Coast of Peru	1988	7	−17.55	−72.83	15	Thrust
Central California	1989	7.1	37.06	−121.63	19	Odd
Macquire Islands	1989	8.3	−52.15	160.41	15	Strike slip
Mindanao, Philippines	1989	7.4	7.88	126.96	36.9	Thrust
Honshu, Japan	1989	7.3	39.93	143.08	24	Thrust
Solomon Islands	1989	7.1	−10.95	162.3	25.2	Odd
Costa Rica	1990	7	9.95	−84.58	17.9	Thrust
Komandorsky Islands	1990	7	53.77	169.41	26.6	Odd
Luzon, Philippines	1990	7.8	15.97	121.23	15	Strike slip
Mariana Islands	1990	7.5	15.57	148.04	15	Normal
Minahassa Peninsula	1990	7.4	1.31	123.35	33.2	Thrust
South of Fiji Islands	1990	7.5	−22.05	175.35	25.3	Strike slip
Sudan	1990	7.2	5.3	32.29	15	Strike slip
Western Iran	1990	7.7	36.95	49.52	15	Odd
Costa Rica	1991	7.5	10.1	−82.77	15	Thrust
Kuril Islands	1991	7.4	45.58	151.55	31.2	Thrust
Colombia	1991	7	4.8	−77.18	19.1	Thrust

Table 1. (continued)

Mainshock	Date	M_s	Latitude	Longitude	Depth (km)	Mainshock Mechanism
Northern India	1991	7.1	30.22	78.24	15	Thrust
Western Caucasus	1991	7	42.6	43.61	22.3	Thrust
Cuba	1992	7	19.84	−77.7	15	Odd
Flores Island Region	1992	7.5	−8.34	122.49	20.4	Thrust
Kyrgyzstan	1992	7.4	42.19	73.32	17	Thrust
Ascension Island	1992	7	−0.71	−12.54	15	Strike slip
Nicaragua	1992	7.2	11.2	−87.81	15	Thrust
Northern Colombia	1992	7.3	7.27	−76.34	15	Odd
Cape Menocino	1992	7.1	40.25	−124.31	15	Thrust
Southern California	1992	7.5	34.65	−116.65	15	Strike slip
Hokkaido, Japan	1993	7.1	43.06	144.29	100	Odd
Hokkaido Japan	1993	7.6	42.71	139.28	16.5	Thrust
Chiapas, Mexico	1993	7.3	14.41	−92.99	29.1	Thrust
off W coast of South Island, New Zealand	1993	7.1	−45.04	166.73	15	Thrust
Mariana Islands	1993	8.1	13.06	145.31	59.3	Thrust
Halmahera, Indonesia	1994	7.2	1.2	127.8	15	Strike slip
Kuril Islands	1994	8.1	43.6	147.63	68.2	Odd
Mindoro Philippines	1994	7.1	13.44	121.32	15	Strike slip
Coast of Peru	1994	7.3	−15.04	−75.37	37.4	Thrust
Honshu, Japan	1994	7.5	40.56	142.99	27.7	Thrust
South Island New Zealand	1994	7.1	−42.94	171.47	15	Odd
South of Java	1994	7.2	−11.03	113.04	15	Thrust
Southern Sumatera	1994	7	−5.15	104.27	16.2	Strike slip
Vanuatu Islands	1994	7.2	−20.45	169.04	42.5	Thrust
Egypt	1995	7.3	29.07	34.73	18.4	Odd
Jalisco, Mexico	1995	7.3	19.34	−104.8	15	Thrust
Antofagasta, Chile	1995	7.3	−24.17	−70.74	28.7	Thrust
Peru-Ecuador Border region	1995	7	−2.55	−77.53	25	Thrust
Sakhalin Island	1995	7.6	53.03	142.65	23.6	Strike slip
Samar, Philippines	1995	7	12.17	126.03	15	Thrust
Solomon Islands	1995	7.8	−5.51	153.64	45.6	Thrust
Tonga Islands	1995	8	−15.37	−173.15	87.9	Odd
Andreanof Islands Aleutians	1996	7.6	51.1	−177.41	29	Thrust
Mnahassa Peninsula	1996	7.7	0.74	119.93	15	Odd
West Irian Region	1996	8.1	−0.67	136.62	15	Thrust
Iran	1997	7.3	33.58	60.02	15	Strike slip
Kamchatka	1997	7.6	54.31	161.91	33.6	Thrust
Pakistan	1997	7.3	29.74	68.13	15.3	Thrust
Tibet	1997	7.9	35.33	86.96	16.4	Strike slip
Balleny Islands	1998	8	−62.99	148.64	28.8	Strike slip
Banda Sea	1998	7	−6.9	128.95	24.6	Thrust
Ceram Sea	1998	7.7	−2.03	125	16.4	Odd
Ecuador	1998	7.7	2.32	−78.81	19.7	Thrust
Papua New Guinea	1998	7.1	−2.5	142.07	15	Thrust
Southeast of Taiwan	1998	7.3	22.37	125.53	22.9	Strike slip
Turkey	1999	7.8	41.01	29.97	17	Strike slip

requirement of choosing the nodal plane that slipped for each event. In order to avoid this complication we use a graphical method developed by *Frohlich* [1992, 2001] which uses the plunge of the P, T, and B-axes (principal stress axes) from the focal mechanism solution to quantitatively display the focal mechanisms on a ternary plot. Using this method to visualize the orientation of the focal mechanism solutions for all of the earthquakes within ±2° of the identified main shocks avoids the complication of having to choose nodal planes for each of the events and allows quantitative observations of small changes in the average focal mechanism before and after the main shock. Each of

Table 2. Thirteen Events That Show a Significant Mean Mechanism Change

Mainshock	Year	M_s	Mechanism	Rotation	Mean Bootstrap Rotation	SD Bootstrap Rotation
Chile (Valparaiso)	1985	7.8	Thrust	0.1568103	0.071088	0.055406
Southern Xinjiang, China	1985	7.6	Odd	0.3268775	0.140187	0.1125747
Andreanof Islands	1986	7.7	Thrust	0.0980941	0.0595034	0.0385797
Central California	1989	7.1	Odd	0.0404359	0.2205444	0.1353424
Komandorsky Islands	1990	7	Odd	0.3266641	0.1795474	0.1243824
Mariana Islands	1990	7.5	Normal	0.2544899	0.1045668	0.0654719
Minahassa Peninsula	1990	7.4	Thrust	0.2075042	0.0484912	0.0402979
Kuril Islands	1991	7.4	Thrust	0.0187813	0.0565789	0.0296271
Western Caucasus	1991	7	Thrust	0.0401338	0.2802456	0.207337
Nicaragua	1992	7.2	Thrust	0.1214096	0.0724194	0.0490826
off W coast of South Island, New Zealand	1993	7.1	Thrust	0.2424798	0.0903928	0.0716335
Egypt	1995	7.3	Odd	0.2379667	0.0422837	0.0981519
Antofagasta, Chile	1995	7.3	Thrust	0.1495336	0.063002	0.0413133

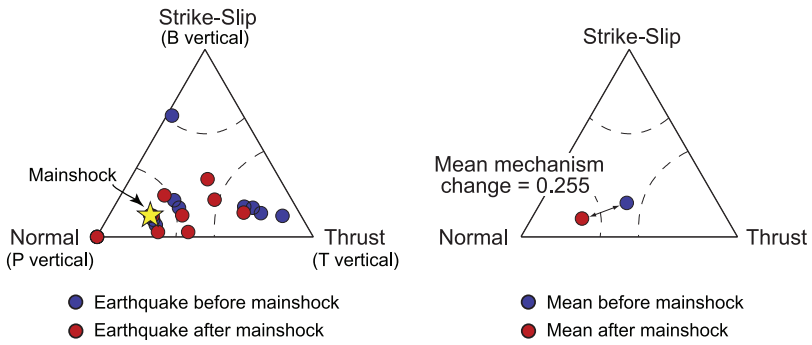

Figure 3. Example of how events are plotted on the ternary plots. The location of the earthquake's mechanism on the ternary plot is determined by the plunge of the *P*-, *T*- and *B*-axes. A pure strike-slip event will have a *B*-axis that is vertical (plunge of 90°) and will plot at the top vertex of the triangle. The dashed lines indicate the limits of each faulting type. The main shock is represented by a yellow star. Events before the main shock are shown as blue dots, while events after the main shock are red dots. For all of the events before and after the main shock, we calculate an average mechanism, which are shown as the blue and red dots in Figure 3a. The mean mechanism change is simply the Euclidean distance between these two mean mechanisms.

the vertices on the ternary plot represents one of the "pure" mechanisms depending on which axis is vertical; thrust when the T-axis is vertical, strike-slip when the B-axis is vertical, and normal when the P-axis is vertical (Figure 3). Following *Frohlich* [1992] we classify focal mechanisms as thrust when the plunge of the P-axis is greater than 50°, and normal or strike-slip when the plunge of the T or B axis is greater than 60°. The typical error on the focal angle from the Harvard CMT catalog is between 0 and 15 degrees and decreases with increasing event depth [*Helffrich*, 1997].

[9] For each identified main shock, the main shock and events within the ±2° box are plotted on a ternary diagram (Figure 3a). The main shock is plotted as a star, the events before the main shock as blue circles, and the events after the main shock as red circles. This allows general observations on the orientation and distribution of focal mechanisms before and after the main shock over the length of the catalog. To identify changes in the average focal mechanisms we calculate the average mechanism before and after the main shock (Figure 3b). The change in average mechanism is quantified by calculating the Euclidean distance between the two average focal mechanisms.

[10] We use a bootstrap analysis to determine the significance of the change in average focal mechanisms following a main shock. Using the 8 years of catalog data before the M > 7 triggering event, we select random 5-year windows and perform the analysis described above to calculate the mean and standard deviation of the average focal mechanism change when there is no triggering event. This requires the assumption that the 8 years before the main shock are representative of the average focal mechanism distribution for the region. If this assumption is correct then the fact that the two 5-year windows overlap will not underestimate the mechanism change with no triggering event. In addition, the two 5-year time windows are drawn independently of each other, that is not requiring that the "before" time window occur earlier in time than the "after" time window, thus allowing for greater variability in the rate changes and focal mechanism rotations. Following the bootstrap iterations, we have a distribution of the variation in average focal mechanisms without a M > 7 triggering event. We use this to determine if the change in average post-shock focal mechanism is significant compared to the variation in mechanism present before the triggering event.

4. Individual Main Shocks

[11] Using the method detailed above we analyzed the 67 M > 7 events in our catalog. This analysis found 13 events with a change in mechanism that is significant at the 1σ level compared to the pre-shock variation (Table 2). We use the lower requirement of 1σ at this early stage in the analysis to increase the number of events we will examine to determine if there is a stress shadow present given the new definition presented above.

[12] Under our definition of a stress shadow, while the overall seismicity rate may increase, we would expect to see a decrease in the rate of at least one mechanism after the main shock to account for the mean change. We thus, look in detail at the evolution of seismicity for each of the mechanisms before and after the main shock for the 13 events that show a significant change (1σ) in the average mechanism following the main shock. For the 13 events that show a significant change in average mechanism we then examine the number of events per year for each mechanism and the annual rate of events for each mechanism during the 5 years before and after the main shock. However, only 2 of the 13 events show a decrease in rate of at least one mechanism which current understanding of dynamic triggering cannot explain. These 2 events also show a change in mechanism that is significant at the 2σ level indicating that the change in mechanism is statistically significant for these events. Figure 4 shows one of the 2 events that have a significant change in the mean mechanism and a decrease in seismicity rate for at least one mechanism; in this case there is a decrease in the number of thrust events. Figure 5 shows an example of an earthquake that caused a significant change in the mean focal mechanism that we do not interpret as a conventional stress shadow. In this example there were rate increases for all mechanisms, but some mechanisms were disproportionately increased such that the mean mechanism changed. Since both the static and dynamic stress triggering

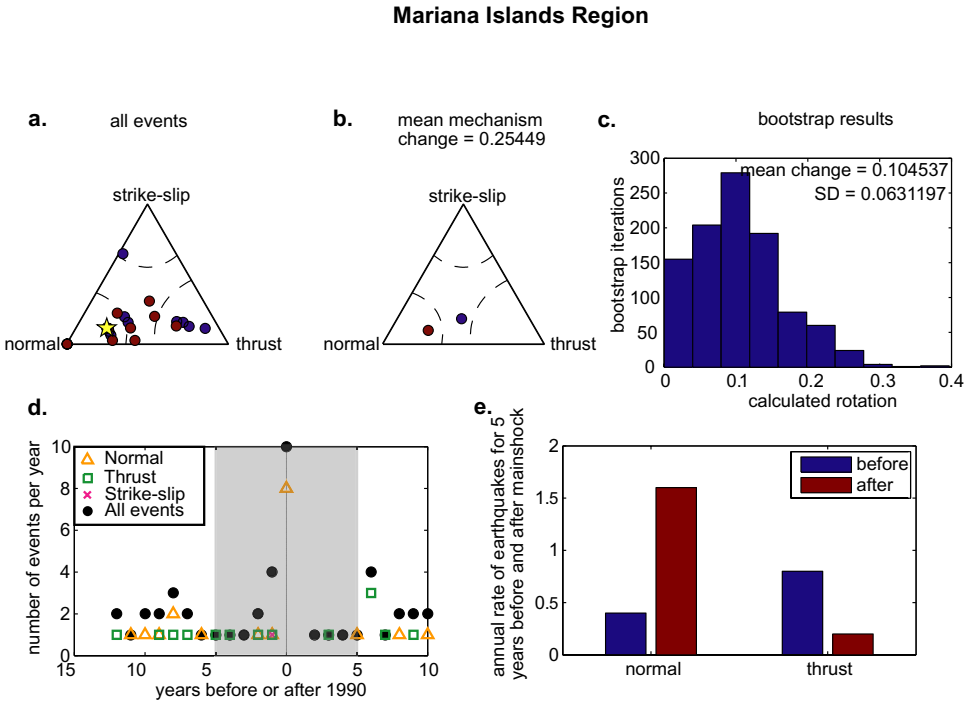

Figure 4. Statistics for the Mariana Islands Region main shock. (a) Ternary plot of the main shock (yellow star), events before (blue dots), and after (red dots) the main shock. There are 9 events in the 5 years before the main shock and 13 in the 5 years after the main shock. (b) The mean mechanism before (blue) and after (red) the main shock and the mean mechanism change. (c) Bootstrap results of the variability of focal mechanism orientation before the main shock with the mean change and standard deviation to test the significance of the observed mechanism change. Bootstrapping was drawn from 22 events before the main shock. (d) Plot of the number of events per year for all mechanisms showing the initial spike in seismicity at the time of the main shock. The grey box indicates the 5 years before and after the main shock, which are used to determine the annual rate of earthquakes. (e) The annual rate of earthquakes for the 5 years before and after the main shock. There is a decrease in the number of thrust events, thus, while there is an overall increase in the number of events after the main shock relative to before, there is a change in the mean mechanism and a decrease of at least one mechanism indicating a stress shadow.

models explain rate increases, this type of mean mechanism change cannot be unambiguously attributed to either the static or dynamic model.

[13] The observation that, for 67 earthquakes of $M_s \geq 7$, only 2 show a decrease in seismicity for any mechanism indicates that stress shadows like the one following the 1906 San Francisco earthquake are rare, or are not identifiable with relatively short data sets (i.e., ±5 years) before and after the $M_s \geq 7$ main shock. In our approach, we assign significant post-earthquake changes to either a static or dynamic cause, thus while these main shocks do not represent a large percentage of the total investigated, they are consistent with static stress shadowing and not dynamic. This observation is important because it suggests that any signal of static stress triggering and especially shadows is subtle. This leads us to consider whether these signals can be extracted by stacking the data.

5. Stacked Data

[14] There appear to be few significant changes in mean earthquake mechanism after individual main shock events in the CMT catalog. However, the 1906 earthquake stress shadow would not have been readily apparent within the first 5 years after the main shock either (the time span of our data). Thus is it possible that stress shadows are present in our catalog, but are sufficiently small such that they are not apparent for individual events. However, by stacking the data we may begin to reinforce the signal. We combine the effects of multiple main shocks to identify any small signals that are not apparent for single events. We create three stacked catalogs grouped by main shock mechanism. Each catalog consists of all of the main shocks of a given mechanism and the associated events within ±2° boxes. For each stacked catalog we align all the main shocks to the same mechanism (arbitrarily chosen to be the central mechanism in the region of the ternary plot for that main shock mechanism). Mechanisms of each earthquake associated with each main shock are changed by the same amount, preserving the relative structural relationships. Once all the main shocks and associated earthquakes are aligned, they can be stacked. We then use these newly stacked catalogs to perform the average mechanism and significance calculations outlined in section 3.

[15] Using the stacked catalogs we determine the number of events per year of each mechanism before and after the

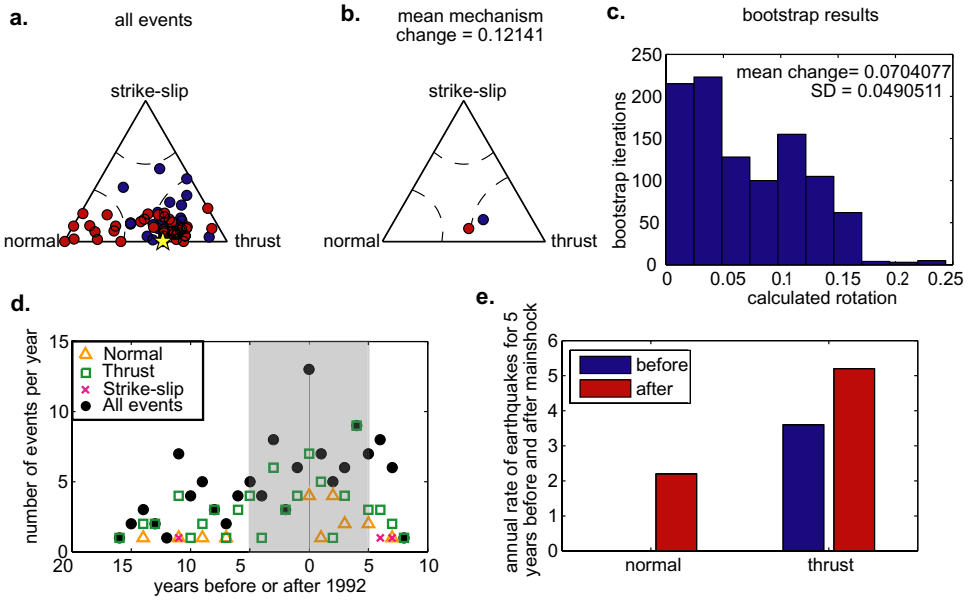

Figure 5. Statistics for the Near Coast of Nicaragua main shock. (a) Ternary plot of the main shock (yellow star), events before (blue dots), and after (red dots) the main shock. There are 32 events in the 5 years before the main shock and 40 events in the 5 years after the main shock. (b) The mean mechanism before (blue) and after (red) the main shock and the mean mechanism change. (c) Bootstrap results of the variability of focal mechanism orientation before the main shock with the mean change and standard deviation to test the significance of the observed mechanism change. The bootstrapping was drawn from 60 events before the main shock. (d) Plot of the number of events per year for all mechanisms showing the initial spike in seismicity at the time of the main shock. The grey box indicates the 5 years before and after the main shock, which are used to determine the annual rate of earthquakes. (e) The annual rate of earthquakes for the 5 years before and after the main shock. There is a decrease in the number of thrust events, thus, while there is an overall increase in the number of events after the main shock relative to before, there is a change in the mean mechanism and a decrease of at least one mechanism indicating a stress shadow. Despite the significant change in mean mechanism, the number of events after the main shock increases for all mechanisms. Where there were no normal events before, there are a substantial number after causing the change in mean mechanism.

main shock (top row of Figure 6). The histograms in Figure 6 illustrate that in all cases, the number of events per year increases following the main shock for all mechanisms. However, one of the benefits of stacking the data is that by increasing the number of events analyzed we are better able to resolve small changes in average mechanism through changes in seismicity rate for submechanisms than would not be apparent for a single main shock. To resolve small changes in average mechanism we grid the ternary diagram into equal 10-degree regions and calculate the difference in the number of earthquakes in the 5 years before and 5 years after the main shock for each stacked catalog. We calculate the rate change in each of the sub-grids in the ternary plot by:

$$\frac{n_a - n_b}{n_a + n_b} \tag{1}$$

where n_a is the number of events after the main shock and n_b is the number of events before the main shock. This gives a number between -1 and $+1$ where the sign indicates whether there is a rate increase (positive) or decrease (negative) and the magnitude of the value indicates the strength of the rate change. The bottom row of Figure 6 shows the results of determining the rate change in the gridded ternary diagram. The presence of blue grid cells indicates that we are beginning to illuminate decreases of certain mechanisms by the main shock. However, we still need to determine if this signal is statistically significant.

[16] To test the significance of the sub-regions of decreased seismicity rate in the gridded ternary plots, we generate two different synthetic stacked catalogs. The first synthetic catalog is generated by randomizing the event times and using the events that fall within 5 years before or after the main shock as before. The second synthetic catalog is generated by randomly pulling events from each main shock's full catalog while maintaining the same number of events before and after the main shock, thus effectively randomizing the event mechanisms while honoring the overall mechanism distribution in each main shock catalog.

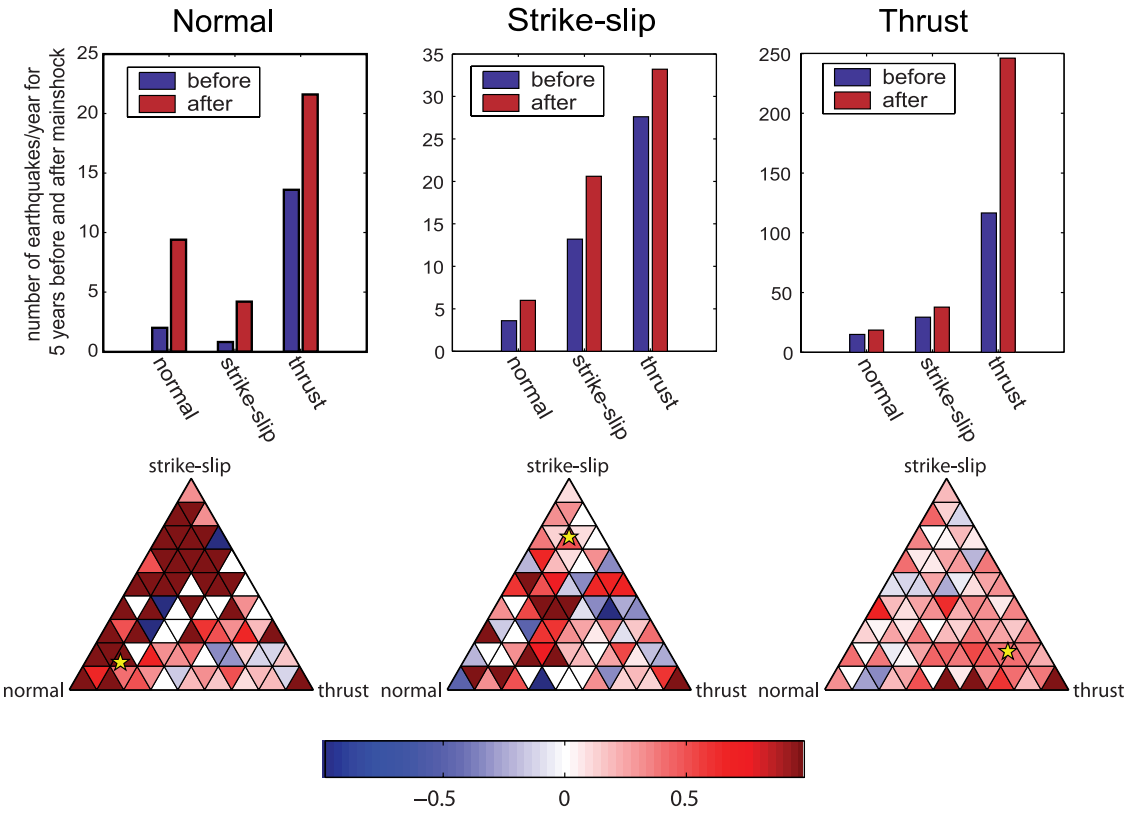

Figure 6. The number of events per year and rate changes for the stacked catalogs. Each catalog consists of main shocks of the same mechanism and all the corresponding seismicity. All the main shocks are aligned to the same mechanism (arbitrarily chosen to be the central mechanism in the region of the ternary plot for that main shock mechanism). Mechanisms of each earthquake associated with each main shock are changed by the same amount, preserving the relative structural relationships and then stacked. The top row shows the number of events per year before and after the main shocks for each main shock mechanism. There is an increase in the number of events per year of all mechanism types following the main shock, but if we look at smaller submechanisms as identified by gridding the ternary plots, decreases in rate of certain mechanisms become evident as is shown in the bottom row. The color in each subtriangle represents the normalized rate change following the main shock as defined by equation (1). Blue represents a decrease in seismicity, while red indicates an increase.

Using the two synthetic catalogs we perform a Monte-Carlo analysis on the variance of the changes in the number of events in a grid cell and the change in average mechanism. The first row of Figure 7 shows the variance of the rate change for the Monte-Carlo analysis on the synthetic catalogs with events randomized in time (light grey) and mechanism (dark grey) with the black line representing the variance for the global catalog. The variance for the global catalog is within the spread of the rate change variances for the synthetic catalogs, indicating that the overall spread of the global catalog is the same as the spread of the synthetic catalogs. This implies that any significant changes in mean mechanism are due to the actual mechanism distribution of events following the main shock.

[17] The change in mean mechanism following the main shock for both the synthetic catalogs and the global catalogs is shown in the bottom row of Figure 7. For all main shock mechanisms the change in average mechanism seen in the global catalog is significant at greater than 95% confidence compared to the synthetic catalogs, though the signal for strike-slip main shocks is smaller than for thrust and normal main shocks. Figure 8 shows the mean mechanisms before and after the main shock for the stacked catalogs plotted on the ternary diagrams. The synthetic catalog changes in mechanism are shown as 1 and 2σ contours around the mean mechanism before the main shock (blue). Again, this plot illustrates that for all three main shock mechanisms, the change in average mechanism following the main shock is significant at 95% confidence, indicating that globally, main shocks do change the average mechanism of events following an earthquake of $M_s \geq 7$. This indicates that while we can't say with confidence that a main shock will suppress earthquakes of a given mechanism, or even of a given submechanism (from the gridded ternary plots), there is a change in the mean mechanism that may be indicative of static stress triggering.

[18] In addition to calculating the rate change in each of the sub-grids using equation (1) and testing the significance as described above, we calculated the significance of the rate change using the z-value [*Habermann*, 1987], β-value [*Matthews and Reasenberg*, 1988] and γ-value [*Marsan and Nalbant*, 2005]. Each of these values calculates the

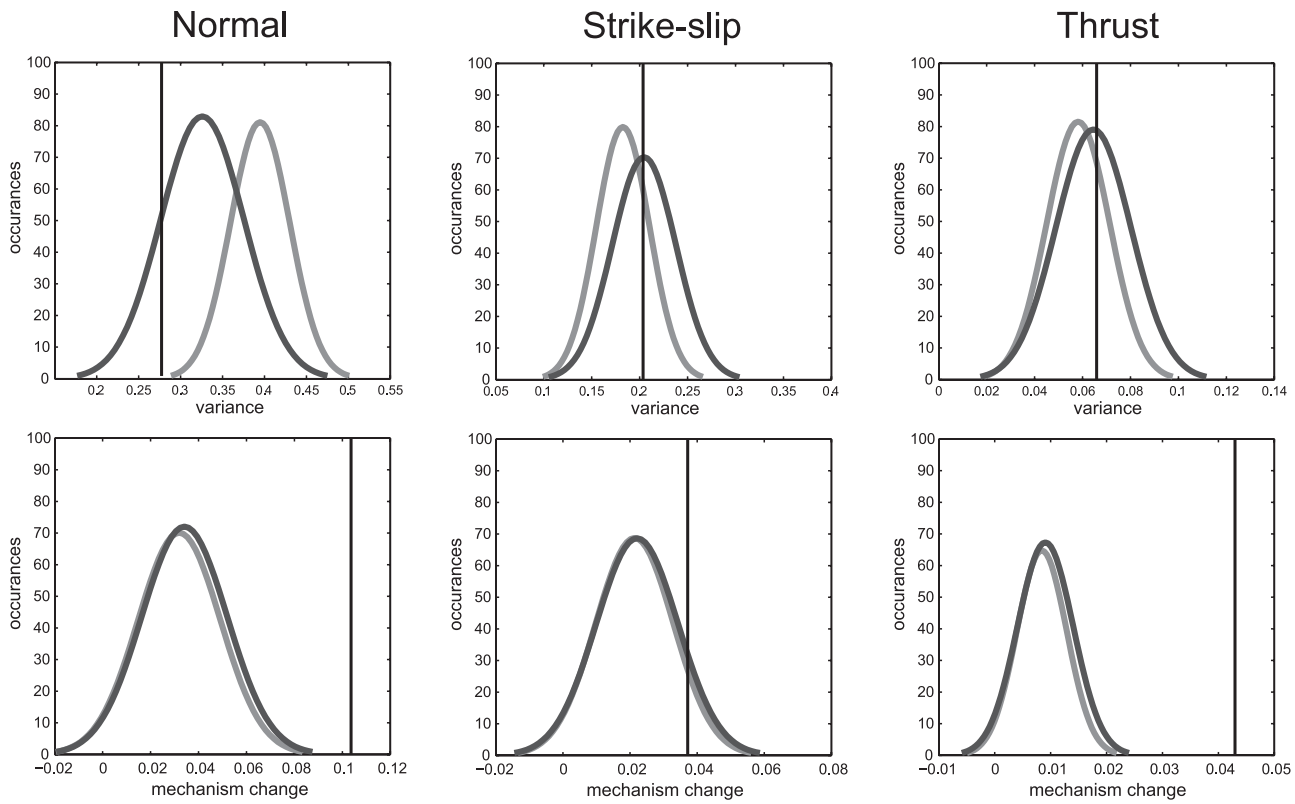

Figure 7. The variance and mean mechanism change for the stacked catalogs compared with Monte Carlo simulations of two synthetic catalogs with events randomized in time (light grey) and mechanism (dark grey). Synthetic catalogs were created using the entire catalog for each main shock. The individual catalogs were then either randomized in time or mechanism and stacked, and the rate and mechanism changes were calculated. The variance is calculated as simply the variance of the rate changes calculated for the subtriangles in the ternary plots shown in the bottom row of Figure 6. The variance for the data falls within the variance for both the synthetic catalogs, indicating that any significant changes to the mechanism are due to the actual distribution of events following the main shock. The bottom row indicates the change in mean mechanism for the data (black line) and the expected distributions of mechanism change for the two synthetic catalogs. For all three stacked catalogs, the change in mean mechanism is significant at the 2σ level.

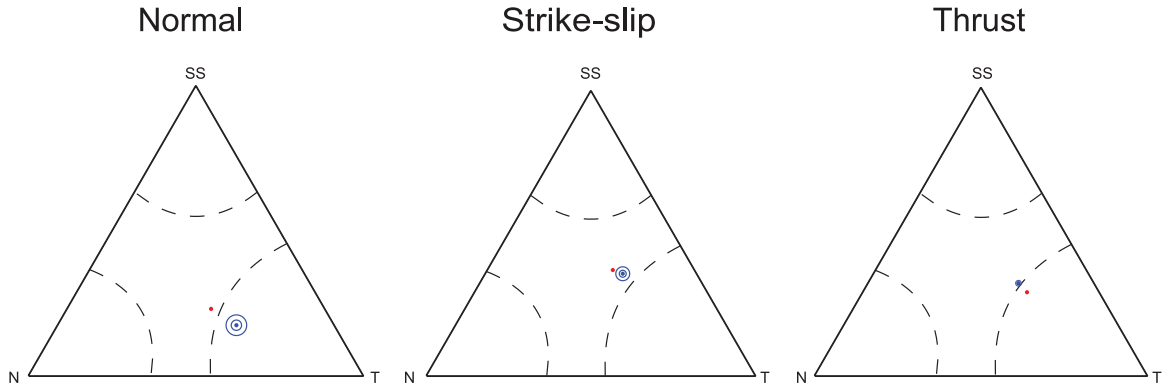

Figure 8. Another way of representing the significance of the change in mechanism for each of the stacked catalogs. The blue and red dots indicate the mean mechanism of the data before and after the main shock, respectively. The 2 blue contours around the mean mechanism before the main shock indicate the 1 and 2σ mechanism changes expected for the synthetic catalogs. In all cases, the observed mechanism changes lie outside the 2σ contour.

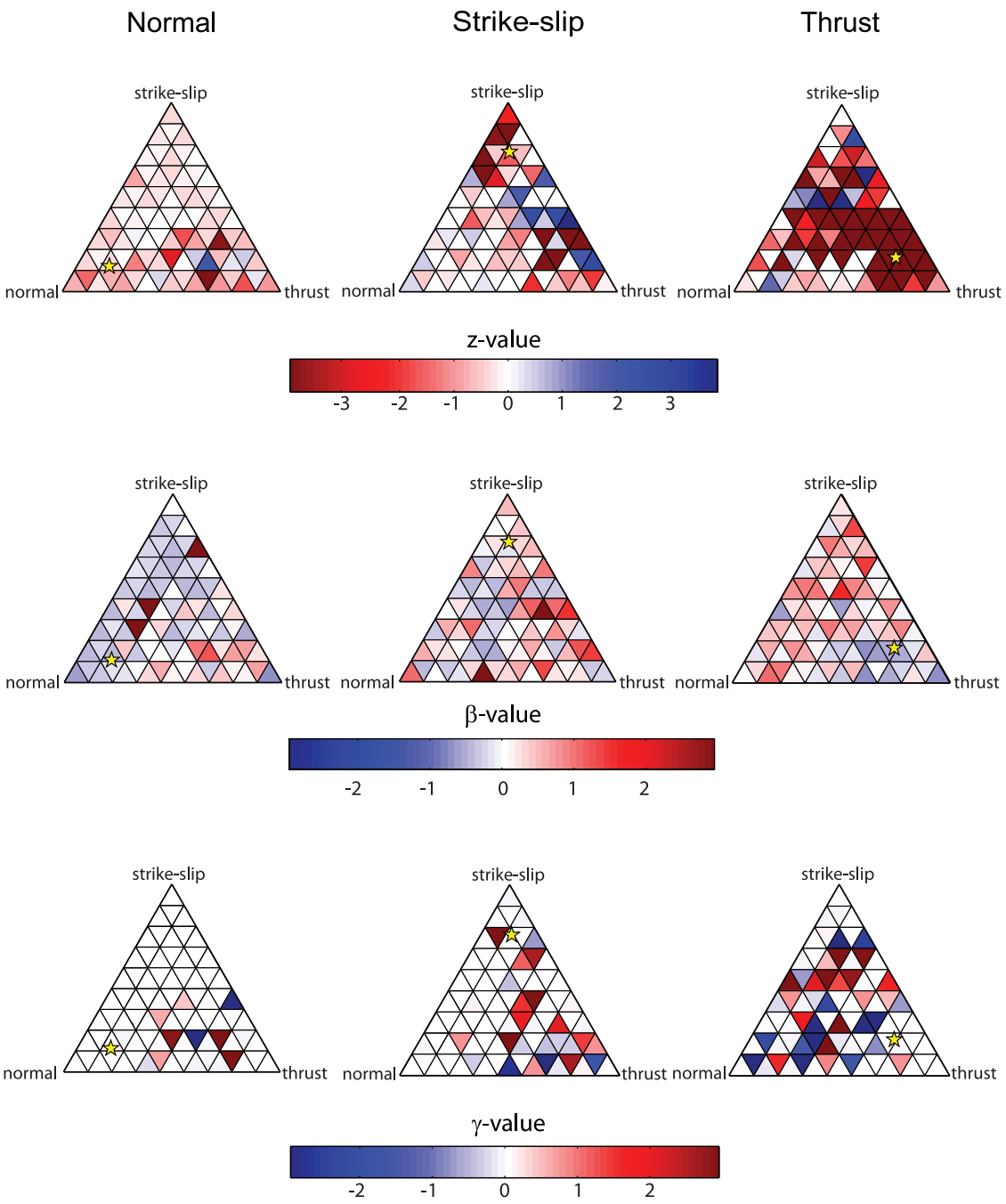

Figure 9. Gridded ternary plots calculating the significance of the seismicity rate changes for the stacked catalog using the z-value, β-value, and γ-value. For all of the plots, seismicity rate increases are indicated by reds and decreases are indicated by blues. The top row shows the rate change using the z-value where values greater than ±1.67 are significant at the 2σ level. The second row shows the rate change using the b-value. Again, values greater than ±1.67 are significant at the 2σ level. The bottom row shows seismicity changes using the g-value. In this case, values greater than ±2 are significant at greater than the 2σ level. Using all 3 measures of significance of seismicity rate change submechanisms experiencing a significant decrease in seismicity rate are able to be resolved. This indicates that the decreases in seismicity rate seen in Figures 6 and 10 are valid.

significance of rate changes between two time periods as opposed to calculating the actual rate change. The significance is based on Poisson (gamma) or Gaussian (z and beta) statistics. Figure 9 shows the significance of the rate changes for the stacked catalogs using each of the values described above with the shades of blue indicating a decrease in the seismicity rate. For both z and β a value of 1.67 indicates 90% significance while for γ a value of 2 indicates 99% significance. All 3 of these statistics show statistically significant rate decreases of certain mecha-

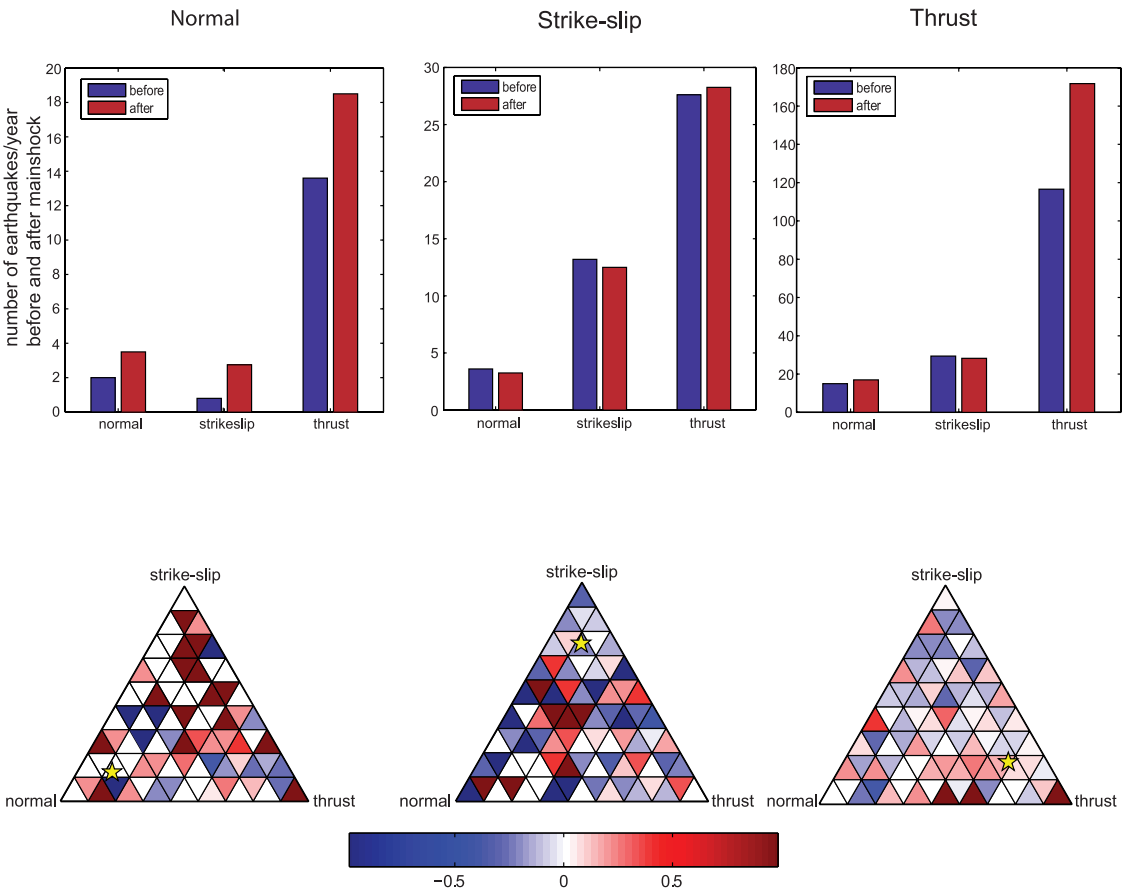

Figure 10. The number of events per year and rate changes for the stacked catalogs excluding the first year following the main shock. The top row shows the number of events per year before and after the main shocks for each main shock mechanism. There are now slight decreases in the number of events of strike-slip and normal events following strike-slip main shocks. The bottom row indicates the change in rate for submechanisms on the ternary plot. The color in each subtriangle represents the normalized rate change following the main shock as defined by equation (1). Blue represents a decrease in seismicity, while red indicates an increase.

nisms. That the z-, β-, and γ- values don't show rate increases and decreases in the same triangles of the gridded ternary plots indicates two things; first, that with small numbers of events to be analyzed, there is an inherent instability to the Poisson and Gaussian statistics, and second, that the change in rate for any given sub-mechanism may not be statistically significant, even if there is a significant change in mean mechanism. This instability and similar conclusions supports our use of equation (1) to define rate change and the synthetic catalogs to determine significance is valid for this study and our conclusions.

[19] An alternative explanation of the observed change in average mechanism following $M_s \geq 7$ main shocks is that some regions were dominated by certain earthquake mechanisms before the main shock, but that after the main shock there are events of all mechanisms. This result could be caused by static or dynamic stress triggering. As an experiment, we eliminate events in the first year following the main shock which may be most affected by dynamic triggering signals. *Parsons* [2002] found that globally, there is a large initial spike in seismicity following a $M_s \geq 7$ main shock that occurs in stress shadow zones that decays back to the background rate in the first year; that population of aftershocks might most readily be explained as dynamically-triggered events. If we remove all events that occurred during the first year after main shocks, are there significant changes in mechanism?

[20] We repeat the analysis on the stacked data after removing events that occurred in the first year following the main shock. The first row of Figure 10 shows the number of events per year before and after the main shock. The seismicity rate increases are substantially smaller than when the first year following the main shock is included (Figures 6 and 10). There remains a modest increase in normal events following normal and thrust main shocks. There is now a small decrease in the average rate of normal and strike-slip events following strike-slip main shocks, though the changes are small enough that their significance is questionable. The bottom row of Figure 10 shows the gridded ternary plots with the colors indicating the change in seismicity rate following the main shock in each sub-grid. In all cases there are more sub-grids that show seismicity rate decreases, but again, the question is whether these

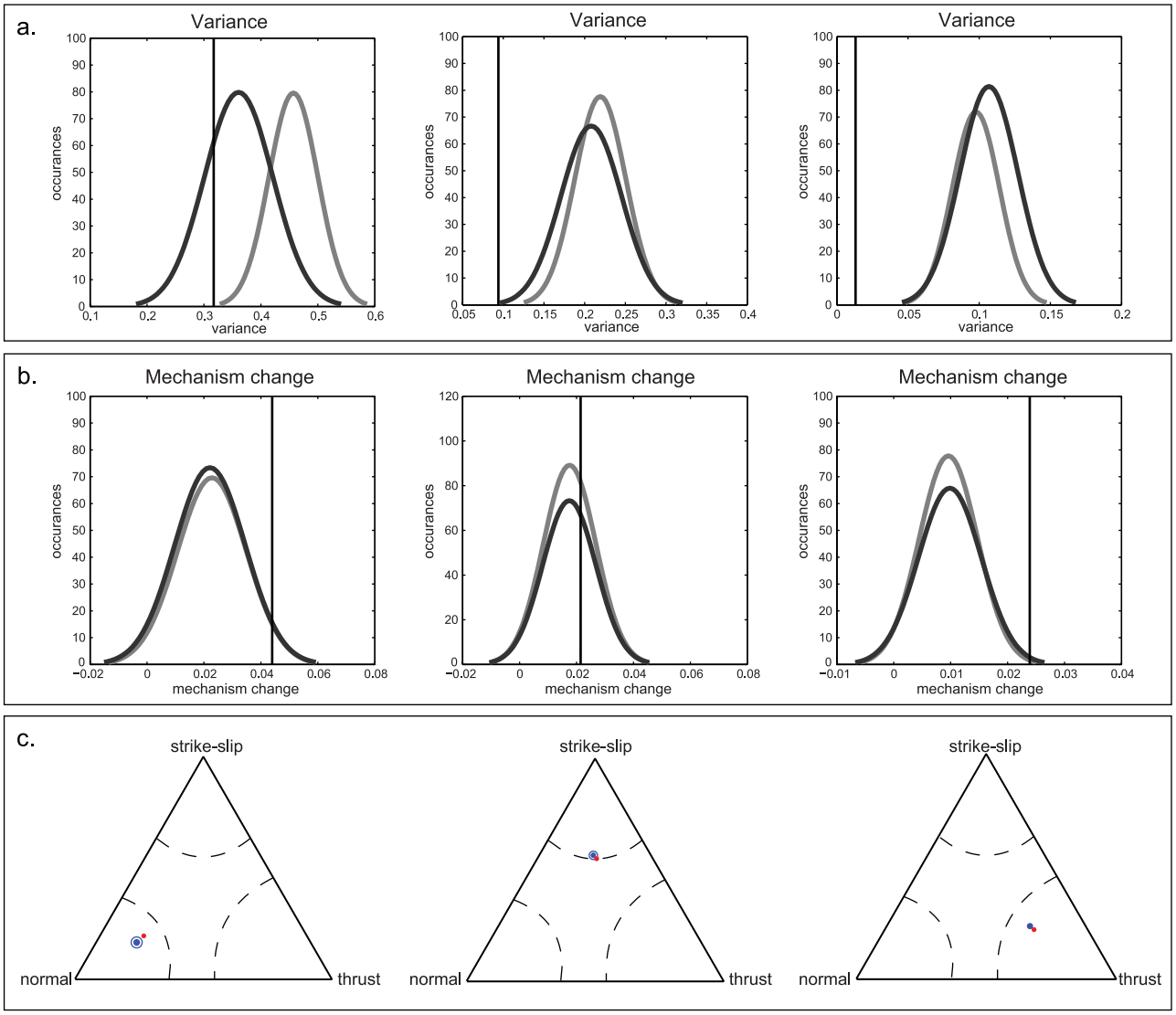

Figure 11. Comparison of the variance and mechanism change for the stacked catalogs excluding the first year following the main shock and the two synthetic catalogs. See captions of Figures 7 and 8 for graphical explanation. Again, the mechanism change observed in the data is significant at the 2σ level over what is expected from the synthetic catalogs.

changes are significant. Figure 11 shows the variance and change in average mechanism for the data (black line) compared to Monte-Carlo analysis for synthetic catalogs randomized in time (dark grey) and mechanism (light grey). Unlike when the first year following the main shock is included, the data variance falls outside the spread of the synthetic catalog variance at 95% confidence in all but one of the cases. However for of the normal and thrust main shock mechanisms the change in average mechanism is significant at the 2σ level, and for the strike-slip main shocks the change in average mechanism is significant at the 1σ level (Figures 11b and 11c).

[21] We also ran the individual main shock analysis from section 4 excluding the first year of data following the main shock. The results were largely similar to including the entire catalog. Out of 67 main shocks analyzed, 14 showed a change in mean mechanism significant at the 1σ level. Of these 14 events, 6 show a decrease in one mechanism type after the main shock, however, most of these decreases are going from 1–2 events before the main shock to none after the main shock. There were only 2 events that showed a marked decrease in one or more mechanism type following the main shock.

[22] Statistically significant changes in the mean mechanism of the stacked catalogs are present whether or not the first year of data following the main shock is included, despite the differences in the variances of the stacked catalogs relative to the synthetic catalogs. This indicates that when the first year of data is included some of the change in mechanism observed is due to turning on events of all mechanisms (i.e., dynamic triggering). However, when the first year of data is removed, the variance of the stacked catalogs is significantly different than that of the synthetic catalogs indicating that any observed change in mechanism is not due to turning on events of all mechanisms, but turning on or off selective mechanism (i.e., static

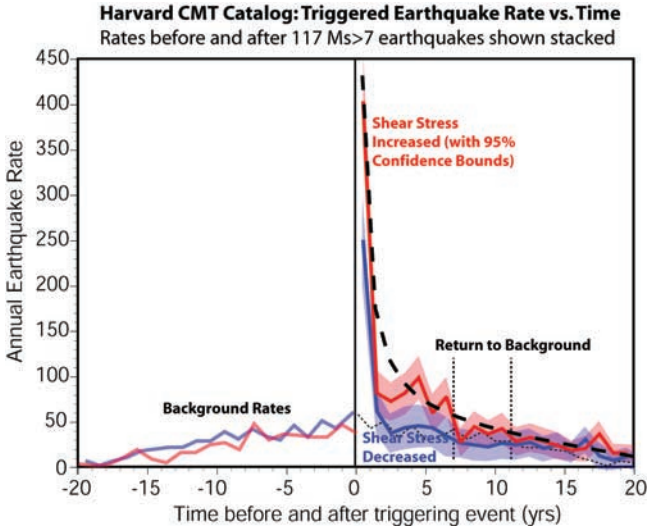

Figure 12. Modified after *Parsons* [2002]. That there is a spike in both number events that see shear stress increases and decreases is indicative of dynamic triggering being a part of the signal. The additional number of events that experience a shear stress increase is likely indicative of changes in static stress. The increases in the blue line drop back to the background quickly, supporting a dynamic mechanism where there are few to no long-term effects on the seismicity rate. The larger increase in the red line can be explained by a combination of both static and dynamic triggering. The initial increase in the red line also drops off quickly as expected for dynamic triggering but remains higher than the background for more than 5 years indicative of static triggering. This overprinting of both static and dynamic effects is likely the reason that stress shadows are very rarely observed for individual earthquakes, and it is only with the stacking of data on a global scale that we are able to begin to resolve them, but even then, the signal is subtle and not the strong 1906-type signal predicted by traditional stress shadow studies.

triggering). Thus it is less likely that the change in mechanism is due to events of all mechanisms being triggered by the main shock since there is a significant change in mean mechanism when the first year of events following the main shock are removed. This indicates that while the signal is very subtle, and superimposed on a dynamic stress triggering signal, the changes in average mechanism following $M_s \geq 7$ are likely indicative of static stress triggering.

6. Discussion

[23] We began this study looking for changes in the mean mechanism of earthquakes associated with individual $M_s \geq 7$ events induced by the main shock that would indicate a stress shadow according to the definition established at the beginning of this paper. Of the 67 main shocks that were identified as potential triggering events, 13 showed a mechanism change significant at the 1σ level. However, only 2 of these 13 events didn't show an over-all increase in seismicity rate across all focal mechanisms. Thus, for only two of the 67 main shocks could a dynamic process not explain observed seismicity rate changes. These two events may exhibit a stress shadow caused by changes in the static stress. This indicates that obvious stress shadows are rare globally.

[24] If stress shadow signals induced by changes in the static stress are subtle, it is possible that the stress shadows are still present, but cannot be resolved for individual events. Using the global catalog of main shocks and their associated events, we stacked the data for each main shock mechanism to amplify any small signals present. The increased number of events allowed us to grid our ternary plots, and examine seismicity rate changes in smaller mechanism bins. We found that statistically significant rate decreases could be resolved for some submechanism bins but there appeared to be no correlation between the submechanisms experiencing rate decreases and the main shock mechanism. However, the changes in average mechanism following the main shock in the stacked data sets were statistically significant. The change in mechanism in the data was significant at the 2σ level compared to synthetic catalogs where the events were randomized in both time and in mechanism.

[25] However, the mean mechanism change in the stacked data sets is accompanied by an increase in the number of events after the main shock for all mechanisms. Thus, it does not fit our new definition of a stress shadow since the change in mean mechanism is not due to a decrease in the number of events of a particular faulting regime. Thus, the mechanism change could be interpreted as dynamic earthquake triggering. If there were very few, or no events of a given mechanism before the main shock, and then after the main shock, events of all mechanisms were increased, there would be a change in the average mechanism. This result could would suggest a dynamic triggering process, but the dynamic triggering could also be masking a static stress triggering signal. By removing the first year of events following the main shock, we limit many of the events that may have been triggered by dynamic stresses. In that instance we observed statistically significant suppression of submechanisms, thus the overall change in mean mechanism may represent static stress shadowing. However, that we can only resolve these changes in average mechanism indicative of a stress shadow after stacking the data indicates that the role of static stresses in changing seismicity rates is very subtle, We thus cannot rule out a hypothesis that the majority of earthquake triggering results from a dynamic process, but we can identify a static stress process operating at some level.

[26] These results are consistent with observations made by *Parsons* [2002] for the evolution of seismicity globally following events $M_s \geq 7$ for regions of static shear stress increase and decrease (Figure 12). The red line indicates events associated with an increase in the shear stress due to the main shock while the blue line indicates events associated with a shear stress decrease. While both lines show a significant spike in seismicity following the main shock followed by an Omori-type decay, the increase in the number of events in areas of shear stress increase is almost twice as large as that for events in areas of shear stress decrease. The observations made by *Parsons* [2002] coupled with the results of this work imply that the increase in rate for events experiencing a shear stress decrease is likely due to dynamic triggering while the increase for events experiencing a

shear stress increase is likely due to both dynamic and static triggering. The difference in the magnitude of the spike in seismicity rate for the regions experiencing shear stress increase versus a shear stress decrease can possibly be attributed to the triggering of events by static stress changes. In addition, the events associated with shear stress decreases drop back to the background seismicity rate in approximately 1–2 years following the main shock while the events associated with shear stress increase take 8–12 years to return to the background rate. The overprinting of both static and dynamic effects likely explains why stress shadows are rarely observed for individual earthquakes. Further, static stress changes caused by slip heterogeneity in the main shocks that was not modeled here or by *Parsons* [2002] is expected to generate isolated zones of seismicity increases within broad shadow zones [*Helmstetter and Shaw*, 2006; *Marsan*, 2006]. Finally, we recognize that different tectonic regimes will have different aftershock durations, and that this may influence the shape of the seismicity decay rate for the stacked catalogs. However, the catalogs can all be stacked because the decay curves all have the same exponential shape. When an aftershock sequence with a shorter decay curve is stacked onto a longer decay curve the shorter sequence will contribute nothing to the overall seismicity rate change after reaching background levels. In addition, we are most concerned with short (±5 year) sequences, and all main shock catalogs have a spike in seismicity at zero time (the time of the main shock). The stacking of seismicity catalogs with differing decay curves would have a much greater impact on this work if we were trying to pick the mean time to return to background rate.

[27] We were required to stack seismicity from a global catalog to overcome these effects and resolve stress shadows. However, the stress shadow signal from the global catalog was still not the strong 1906-type signal that often informs our thinking, although with only a ±5-year observation period as we've applied in this study, we might have had a difficult time identifying the 1906 shadow, the impact of which is most evident over ±75 year periods [*Bakun*, 1999; *Stein*, 1999]. Instead we observe changes in average mechanism, which might be a more typical form of stress shadow.

[28] Our observation that the static signal is very subtle and requires stacking of many events to resolve is consistent with work by *Pollitz and Johnston* [2006]. Examining aftershock rates associated with both impulsive and aseismic M∼5 events near San Juan Batista, CA, *Pollitz and Johnston* [2006] find that the impulsive events trigger much higher aftershock activity. As the moment release of the impulsive and aseismic events is roughly equivalent, they attribute the difference in aftershock rate to the dynamic stresses following the impulsive events, which the aseismic events lack. Another mechanism for explaining subtle or delayed stress shadows is the heterogeneity of the stress field following the main shock [*Marsan*, 2006]. This mechanism can be particularly important close to the main rupture plane where slip is heterogeneous. In addition, this may explain why stress shadow signals like the one following the 1906 San Francisco earthquake are so difficult to identify using a smooth slip distribution as is typical for CFS modeling. The effect of stress heterogeneity on stress shadows does not disprove the conclusions of *Pollitz and Johnston* [2006], and is beyond the scope of this work as we do not have or consider the rupture models of stress fields of the 67 events analyzed.

[29] It is commonly recognized that current models of changes in static Coulomb stress following an individual main shock cannot reproduce the on-fault aftershocks which can dominate the catalog. Generally, these studies have removed the aftershocks within a certain distance of the main shock rupture [*Mallman and Zoback*, 2007; *Toda et al.*, 1998] However, in theory a global catalog will have a mixture of on and off-fault aftershocks which may increase the tendency toward resolving seismicity rate increases. We find that in our global catalog very few of the aftershocks studied are located along the rupture plane of the main shock indicating that the on-fault aftershocks do not have a large impact on the seismicity rate changes we observe.

[30] Clearly identified stress shadows, similar to the one observed following the 1906 San Francisco earthquake, appear to be rare globally. However, the 1906 shadow was observed as a decrease in the number of M = 6 events and took decades to become apparent, much longer than our catalog data. Thus it could be argued that not seeing stress shadows for individual events in our catalog is not an indication of the lack of stress shadows, but that our catalog is too short to identify the change in seismicity rate. It is also possible that if the catalog following the 1906 earthquake were complete down to M = 4, the stress shadow would have become apparent earlier due to the greater number of background M = 4 and 5 events compared to M = 6 events. In addition, the 1906 San Francisco earthquake was unusual in that it was an extremely long strike-slip rupture with most of the regional faults sub-parallel to the rupture, reducing the static stress on most of the active faults in the region. Since the global catalog is dominated by thrust events, and events with ruptures much shorter than the rupture of the San Andreas Fault in 1906 it isn't surprising that we don't see many seismicity rate reductions following $M_s \geq 7$ events globally, and in fact the lack of rate reductions does not appear to be very diagnostic of stress shadows after all. Instead, we suggest that static triggering (and thus, shadows) does occur by the demonstration of a mean mechanism change following the main shock. This indicates that while the static signal is very subtle and is generally not resolvable until many events are stacked; the static stress model for earthquake triggering and suppression cannot be excluded.

7. Conclusions

[31] Globally we find that out of 67 testable main shocks, only 2 show changes in seismicity rate and average mechanism that cannot be explained by dynamic effects. However, by stacking all the events by the main shock type and gridding associated earthquakes by mechanism, there do appear to be submechanisms that show decreases in seismicity following the main shock. There is a significant change in the mean mechanism following the main shock for the 5 years following the main shock, and for some submechanisms when the first post-main shock year is excluded. We thus conclude that by stacking the global data we are beginning to resolve potential stress shadows which are not identifiable for most main shocks taken

individually due to their subtle nature. In addition, since for none of the 67 main shocks $M_s \geq 7$ examined was there a traditionally defined stress shadow, a decrease in overall seismicity similar to what was observed post-1906, appears to be very rare, at least on the timescales of most seismicity catalogs. While over longer time periods decreases in seismicity similar to those observed following the 1906 San Francisco earthquake may be present, the blanket assumption that seismic risk is lower in the years following a major earthquake may not be accurate. In this work we have been able to identify very subtle signals of static stress shadows, indicating that stress shadows may need to be incorporated into hazard calculations. However, the more conservative hazard estimates would benefit from not assuming there will be a decrease in seismic hazard following major earthquakes as the stress shadow signals found in this study were very subtle on a 5 year timescale.

[32] **Acknowledgments.** Thank you to Paul Hagin, Mark Zoback, David Marsan, Shiji Toda, and Karen Felzer for their critical reviews of this article, which improved it greatly.

References

Bakun, W. H. (1999), Seismicity activity of San Francisco Bay region, *Bull. Seismol. Soc. Am.*, *89*, 764–784.

Belardinelli, M. E., et al. (1999), Redistribution of dynamic stress during coseismic ruptures: Evidence for fault interaction and earthquake triggering, *J. Geophys. Res.*, *104*, 14,925–14,945.

Cotton, F., and O. Coutant (1997), Dynamic stress variations due to shear faults in a plane-layered medium, *Geophys. J. Int.*, *128*, 676–688.

Das, S., and C. H. Scholz (1981), Off-fault aftershock clusters caused by shear stress increase?, *Bull. Seismol. Soc. Am.*, *71*, 1669–1675.

Dziewonski, A. M., et al. (1981), Determination of earthquake source parameters from waveform data for studies of global and regional seismicity, *J. Geophys. Res.*, *86*, 2825–2852.

Felzer, K. R., and E. E. Brodsky (2005), Testing the stress shadow hypothesis, *J. Geophys. Res.*, *110*, B05509, doi:10.1029/2004JB003277.

Felzer, K. R., et al. (2002), Triggering of the 1999 M_w 7.1 Hector Mine earthquake by aftershocks of the 1992 M_w 7.3 Landers earthquake, *J. Geophys. Res.*, *107*(B9), 2109, doi:10.1029/2001JB000911.

Felzer, K. R., et al. (2004), A common origin for aftershocks, foreshocks, and multiplets, *Bull. Seismol. Soc. Am.*, *93*, 88–98.

Freed, A. M., and J. Lin (2001), Delayed triggering of the 1999 Hector Mine earthquake by viscoelastic stress transfer, *Nature*, *411*, 180–183.

Frohlich, C. (1992), Triangle diagrams: Ternary graphs to display similarity and diversity of earthquake focal mechanisms, *Phys. Earth Planet. Inter.*, *75*, 193–198.

Frohlich, C. (2001), Display and quantitative assessment of distributions of earthquake focal mechanisms, *Geophys. J. Int.*, *144*, 300–308.

Gomberg, J., et al. (2001), Earthquake triggering by seismic waves following Landers and Hector Mine earthquakes, *Nature*, *411*, 462–466.

Gomberg, J., et al. (2003), Observing earthquakes triggered in the near field by dynamic deformations, *Bull. Seismol. Soc. Am.*, *93*, 118–138.

Habermann, R. E. (1987), Man-made changes in seismicity rates, *Bull. Seismol. Soc. Am.*, *77*, 141–159.

Harris, R. A., and R. W. Simpson (1998), Suppression of large earthquakes by stress shadows: A comparison of Coulomb and rate-and-state failure, *J. Geophys. Res.*, *103*, 24,439–24,451.

Helffrich, G. R. (1997), How good are routinely determined focal mechanisms? Empirical statistics based on a comparison of Harvard, USGS and ERI moment tensors, *Geophys. J. Int.*, *131*, 741–750.

Helmstetter, A., and B. E. Shaw (2006), Relation between stress heterogeneity and aftershock rate in the rate-and-state model, *J. Geophys. Res.*, *111*, B07304, doi:10.1029/2005JB004077.

Kilb, D., et al. (2000), Triggering of earthquake aftershocks by dynamic stresses, *Nature*, *408*, 570–574.

King, G. C. P., et al. (1994), Static stress changes and the triggering of earthquakes, *Bull. Seismol. Soc. Am.*, *84*, 935–953.

Lin, J., and R. S. Stein (2004), Stress triggering in thrust and subduction earthquakes and stress interaction between the southern San Andreas and nearby thrust and strike-slip faults, *J. Geophys. Res.*, *109*, B02303, doi:10.1029/2003JB002607.

Ma, J.-F., et al. (2005), Response of seismicity to Coulomb stress triggers and shadows of the 1999 Mw = 7.6 Chi-Chi, Taiwan, earthquake, *J. Geophys. Res.*, *110*, B05S19, doi:10.1029/2004JB003389.

Mallman, E. P., and M. D. Zoback (2007), Assessing elastic Coulomb stress transfer models using seismicity rates in southern California and southwestern Japan, *J. Geophys. Res.*, *112*, B03304, doi:10.1029/2005JB004076.

Marsan, D. (2006), Can coseismic stress variability suppress seismicity shadows? Insights from a rate-and-state friction model, *J. Geophys. Res.*, *111*, B06305, doi:10.1029/2005JB004060.

Marsan, D., and S. S. Nalbant (2005), Methods for measuring seismicity rate changes: A review and a study of how the Mw 7.3 Landers earthquake affected the aftershock sequence of the Mw 6.1 Joshua Tree earthquake, *Pure Appl. Geophys.*, *162*, 1151–1185, doi:1110.1007/s00024-00004-02665-00024.

Masterlark, T., and H. F. Wang (2002), Transient stress-coupling between the 1992 Landers and 1999 Hector Mine, California, earthquakes, *Bull. Seismol. Soc. Am.*, *92*, 1470–1486.

Matthews, M. V., and P. A. Reasenberg (1988), Statistical methods for investigating quiescence and other temporal seismicity patterns, *Pageoph*, *126*, 357–372.

Meltzner, A. J., and D. J. Wald (2003), Aftershocks and triggered events of the Great 1906 California earthquake, *Bull. Seismol. Soc. Am.*, *93*, 2160–2186.

Parsons, T. (2002), Global Omori law decay of triggered earthquakes: Large aftershocks outside the classical aftershock zone, *J. Geophys. Res.*, *107*(B9), 2199, doi:10.1029/2001JB000646.

Parsons, T. (2005), Significance of stress transfer in time-dependent earthquake probability calculations, *J. Geophys. Res.*, *110*, B05S02, doi:10.1029/2004JB003190.

Pollitz, F., and I. S. Sacks (2002), Stress triggering of the 1999 Hector Mine earthquake by transient deformation following the 1992 Landers earthquake, *Bull. Seismol. Soc. Am.*, *92*, 1487–1496.

Pollitz, F., and M. J. S. Johnston (2006), Direct test of static stress versus dynamic stress triggering of aftershocks, *Geophys. Res. Lett.*, *33*, L15318, doi:10.1029/2006GL026764.

Reasenberg, P. A., and R. W. Simpson (1992), Response of regional seismicity to the static stress change produced by the Loma Prieta earthquake, *Science*, *255*, 1687–1690.

Richardson, E., and C. Marone (1999), Effects of normal stress vibrations on frictional healing, *J. Geophys. Res.*, *104*, 28,857–28,878.

Simpson, R. W., and P. A. Reasenberg (1994), Earthquake-induced static-stress changes on central California faults, in *The Loma Prieta, California, Earthquake of 17 October 1989 - Tectonic Processes and Models*, edited by R. W. Simpson, pp. 55–89, USGS Professional Paper 1550-F.

Stein, R. S. (1999), The role of stress transfer in earthquake occurrence, *Nature*, *402*, 605–609.

Stein, R., and M. Lisowski (1983), The 1979 Homestead Valley earthquake sequence, California; control of aftershocks and postseismic deformation, *J. Geophys. Res.*, *88*, 6477–6490.

Toda, S., et al. (1998), Stress transferred by the 1995 Mw = 6.9 Kobe, Japan, shock: Effect on aftershocks and future earthquake probabilities, *J. Geophys. Res.*, *103*, 24,543–24,565.

Woessner, J., et al. (2004), The 1997 Kagoshima (Japan) earthquake doublet: A quantitative analysis of aftershock rate changes, *Geophys. Res. Lett.*, *31*, L03605, doi:10.1029/2003GL018858.

Working Group on California Earthquake Probabilities (2003), Earthquake Probabilities in the San Francisco Bay Region: 2002–2031, *U.S. Geologcial Survey Open-File Report 03-214*.

Wyss, M., and S. Wiemer (2000), Change in the probability for earthquakes in Southern California due to the Landers magnitude 7.3 earthquake, *Science*, *290*, 1334–1338.

Yamashina, K. (1978), Induced earthquakes in the Izu Peninsula by the Izu-Hanto-oki earthquake of 1974, Japan, *Tectonophysics*, *51*, 139–154.

E. P. Mallman, Department of Geophysics, Stanford University, 397 Panama Mall, Mitchell Building 360, Stanford, CA 94305-2115, USA. (ellen.mallman@bp.com)

T. Parsons, U.S. Geological Survey MS-999, 345 Middlefield Road, Menlo Park, CA 94025, USA. (tparsons@usgs.gov)